



OPEN ACCESS

EDITED BY

Tabish Alam,
Central Building Research Institute (CSIR),
India

REVIEWED BY

Dariusz Butrymowicz,
Bialystok University of Technology,
Poland

Vipin Shrivastava,
Lakshmi Narain College of Technology,
India

*CORRESPONDENCE

Abdelaziz Nasr,
✉ ahnasr@uqu.edu.sa

RECEIVED 19 January 2023

ACCEPTED 17 April 2023

PUBLISHED 22 May 2023

CITATION

Nasr A, Nassif A and Al-Ghamdi AS (2023),
Binary liquid film condensation from
water-ammonia vapors mixture flowing
downward along a parallel
plate condenser.
Front. Mech. Eng 9:1148246.
doi: 10.3389/fmech.2023.1148246

COPYRIGHT

© 2023 Nasr, Nassif and Al-Ghamdi. This is an open-access article distributed under the terms of the [Creative Commons Attribution License \(CC BY\)](#). The use, distribution or reproduction in other forums is permitted, provided the original author(s) and the copyright owner(s) are credited and that the original publication in this journal is cited, in accordance with accepted academic practice. No use, distribution or reproduction is permitted which does not comply with these terms.

Binary liquid film condensation from water-ammonia vapors mixture flowing downward along a parallel plate condenser

Abdelaziz Nasr*, Ahmed Nassif and Abdulmajeed S. Al-Ghamdi

Mechanical Engineering Department, College of Engineering and Islamic Architecture, Umm Al-Qura University, Makkah, Saudi Arabia

The ammonia-water film condensation is used as an efficient working fluid in industrial applications such as refrigeration, plate condenser and evaporator, absorber/generator heat exchange, air-conditioning, heat pumps and separation processes. The present work focuses on a numerical investigation of water-ammonia condensation on a falling binary liquid film inside a parallel plate condenser by mixed convection. The parallel plate condenser is composed by two parallel vertical plates. One of the plates is wetted by liquid film and cooled by the thermal flux cooling while the other plate is isothermal and dry. Parametric computations were performed to investigate the effects of the inlet parameters of gas, the properties of the binary liquid film as well as the thermal flux cooling on the combined mass and heat transfer and on the efficiency of the parallel plate condenser. The results show that an increase in the inlet vapor of ammonia as well as of vapor water enhances the efficiency of the parallel plate condenser. It is shown also that an enhancement of efficiency of the parallel plate condenser has been recorded when the thermal flux cooling and inlet liquid flow rate is elevated. Whereas the increase of the inlet liquid concentration of ammonia inhibits the efficiency of the parallel plate condenser.

KEYWORDS

water-ammonia mixture, condensation, heat and mass transfer, mixed convection, binary liquid film

1 Introduction

The mixture vapors condensation is found in many industrial applications such as condenser, condensing devices, air-conditioning, refrigeration technology, absorber/generator heat exchange, nuclear technology and separation processes. The studies concern the case of mixture condensation are presented in (Akiyama et al., 2001; Kuchma et al., 2011; Kuchma et al., 2013; Zheng et al., 2019; Wang et al., 2020; George et al., 2022; Hughes and Chen, 2022). Akiyama et al. (2001) presented a numerical simulation of the water-ethanol condensation on a horizontal wall in a plane two-dimensional field. Hughes and Chen (2022) presented a machine learning regression models to predict the heat transfer coefficient and frictional pressure gradient during condensation of three zeotropic mixtures. Kuchma et al. (2011) studied the droplet composition and the droplet size as functions of time at small deviations from the stationary concentration in the growing droplet. (Kuchma et al. (2013) considered the transient stage of evolution in size, temperature and composition of a droplet, which non isothermally condenses or evaporates in the diffusion or free-molecular regime in the atmosphere of two

condensable vapors and neutral carrier gas. George et al. (2022) showed that the efficiency of heat transfer in DWC depends on the heat transfer rates of individual droplets and the droplet size distribution. Wang et al. (2020) presented an experimental system was designed and built to study the Marangoni condensation of ethanol–water mixtures on a horizontal surface, and the growth of condensate droplets during the time-series process. Zheng et al. (2019) proposed a distributed point sinks method (DPSM) for capturing the strong interaction during dropwise condensation because of a large number of the droplets and the closer inter-droplet spacing. A model of laminar pure film condensation from zeotropic binary mixtures in a vertical tube was developed by Le et al. (2022). It was found that the layer thickness and liquid thermal conductivity have an important effect on the local heat transfer coefficient. They showed that the local heat transfer coefficient increased with an increase in the mass fraction of the less condensable component. A numerical analysis of the laminar film condensation of vapor-gas mixtures in horizontal channels has been investigated by Siow et al. (2002). They examined how the film thickness and heat and mass transfers were affected by the gas concentration, Reynolds number, pressure, and the temperature difference from the intake to the wall. The pure liquid film condensation of vapor flowing in a vertical tube and between parallel plates has been treated by Panday (2003). They presented the heat transfer coefficient for the condensation of the R123/R134a vapour mixture as well as the heat flow rate for the condensation of R123. Li et al. (2022) presented a numerical model for the binary zeotropic mixture condensation. They presented a numerical model for the heat transfer coefficients from the experimental data. Wu et al. (2020) conducted a theoretical model of heat transfer during pure liquid film condensation inside the tube. They considered the effect of gravity, viscous force and centrifugal force on the film liquid condensation heat transfer. Liu et al. (2020) presented a theoretical study of laminar pure film condensation inside and outside vertical channels. They showed an enhancement of the condensation heat transfer coefficient on both inside and outside converging channels. However, they showed that the use of the diverging channels deteriorates the condensation heat transfer coefficient. Nasr (2018) numerically treated the pure liquid film condensation flowing down on a vertical channel coated with a porous layer. The author showed that the liquid film condensation is enhanced with the presence of the porous layer. Nasr and Al-Ghamdi (2017) presented a study of the pure film evaporation by natural convection in the presence of porous layer. They developed a heat transfer correlation of the experimental data during liquid film condensation under natural convection. They showed that the presence of the porous layer enhances the heat and mass transfer with liquid-film evaporation. Varier et al. (2022) presented an experimental work of multi-effect solar still and air gap distillation technologies. Berto et al. (2022) developed a several models during experimental study of pure liquid film condensation in microgravity. A numerical analysis of liquid film condensation on porous surface within ceramic membrane has been done by Yang et al. (2023). They showed that the numerical simulations have agreed with experimental results on a same size micro-porous ceramic membrane. Chang et al. (2021) conducted a film condensation heat transfer of low-mass-flux steam and high-pressure in inclined tube. They presented the effect of each parameter on the

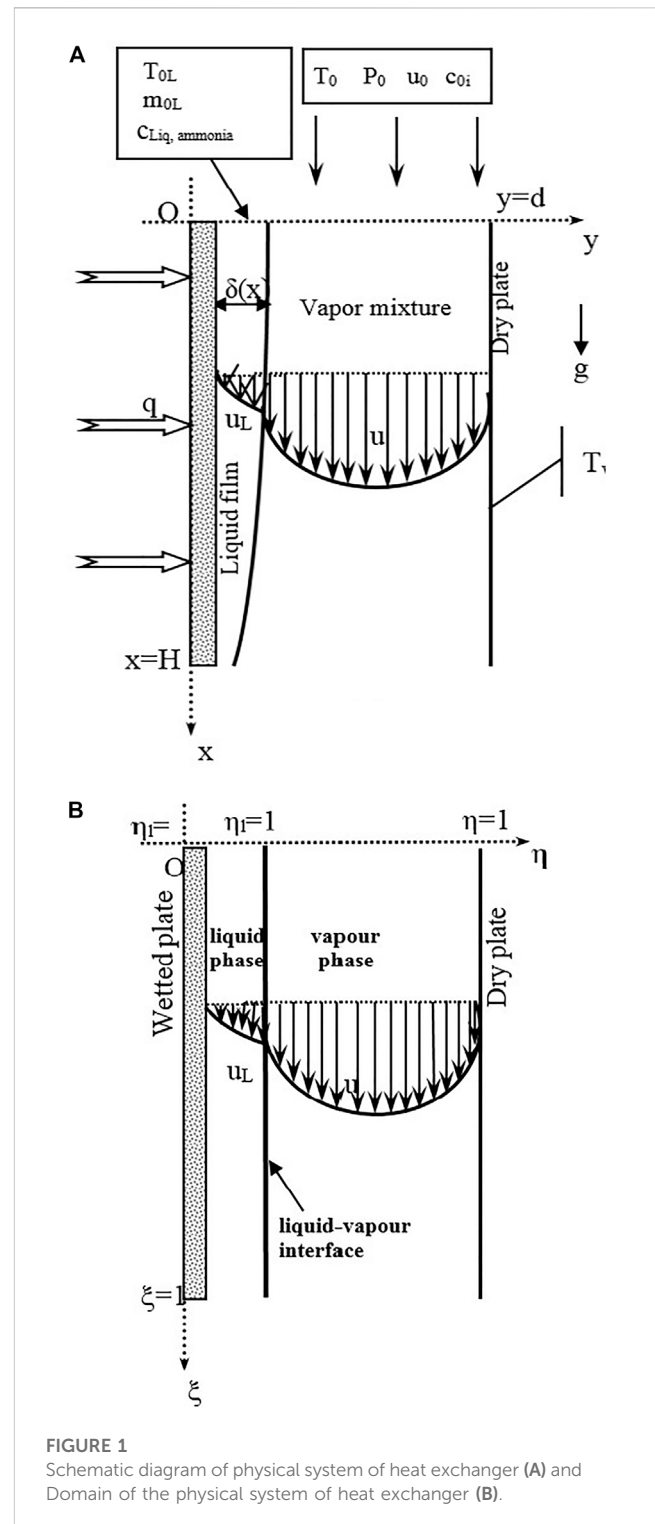


FIGURE 1
Schematic diagram of physical system of heat exchanger (A) and Domain of the physical system of heat exchanger (B).

film condensation using the average heat transfer coefficients. Lee et al. (2022) presented a computational fluid dynamics (CFD) of the wall film condensation in the presence of non-condensable gases. Wang et al. (2018) presented a theoretical model of pure film condensation flow in oval microchannels. They presented the mean heat transfer coefficient and the local heat transfer coefficient along the flow direction. Turkyilmazoglu (2017) examined the liquid film condensation over curved vertical walls.

TABLE 1 Comparison of local evaporating rate (10^5 Mr) ($\text{kg}\cdot\text{s}^{-1}\cdot\text{m}^{-2}$) for various grid arrangements for $T_0 = 20^\circ\text{C}$, $T_w = 20^\circ\text{C}$, $T_{OL} = 10^\circ\text{C}$, $m_{OL} = 0.001 \text{ kg/m}\cdot\text{s}$, $q_1 = 0$, $p_0 = 9 \text{ atm}$, $c_{O1} = 0$, $c_{O2} = 0 \text{ d/H} = 0.015$, $u_0 = 0.75 \text{ m/s}$.

IxJxK grid point	x = 0.2	x = 0.4	x = 0.6	x = 0.8	x = 1
51x(51 + 31)	13.4607	19.8265	24.9689	30.4598	35.8032
101x(51 + 31)	13.3546	19.7192	24.7733	30.5067	35.9063
101x(31 + 31)	13.5511	19.9013	24.5764	30.4485	35.8801
101x(51 + 51)	13.7518	19.8017	24.6978	30.6153	35.8519
151x(51 + 51)	13.1332	19.6986	24.9041	30.53%	35.9105

I: total grid points in the axial direction; J: total grid points in the transverse direction in the gaseous phase; K: total grid points in the transverse direction in the liquid phase.

It is shown that, in the presence of nanoparticles, the heat transfer is more enhanced in the two-phase model case compared to the one phase model case. A numerical and analytical analysis of the film condensation on the wall of an inclined porous plate was provided by [Chaynane et al. \(2004\)](#). The comparison of the Darcy-Brinkman-Forchheimer (DBF) model and the Darcy-Brinkman (DB) model has been treated. Additionally, they discussed the impact of the dimensionless thickness of porous coating, permeability and the effective viscosity on the heat and flow transfer. A numerical analysis of the laminar film condensation over an inclined channel with an insulated upper wall and an isothermal wall coated with a thin porous material was provided by [Merouani et al. \(1993\)](#). For various operating conditions, they displayed the axial evolution of the condensate flow rate and the wall heat flux. They provided that the porous layer properties have a negligible effects on the film condensation compared to the Reynolds number, the inclination angle and the relative humidity. Minkowycz and Sparrow’s study ([Minkowycz and Sparrows, 1969](#)) on the condensation of pure vapors on plates is one of the most significant studies. Theoretical research on falling film condensation caused by free convection on an isothermal vertical plate has been presented. They showed the significance of non-condensable gas impact at lower pressure levels. The experimental study of the liquid film and drop condensation has been presented by [Chung et al. \(2004\)](#). They reveals that the heat transfer rates of drop condensations are significantly higher than those of film condensations in the cases of pure steam. The liquid film condensation of a saturated vapor on an inclined plate embedded in a porous medium has been treated by [Renken et al. \(1993\)](#). They examined the effect of the presence of porous metallic coating on the film condensation.

This literature review shows that the problem of the numerical study of the water-ammonia binary liquid film condensation flowing downward along a parallel plate condenser has not been studied. The purpose of this paper is to discuss the effects of the inlet parameters of the gas mixture and of the liquid mixture film on the heat and mass transfer and on the total cumulated condensation rate of water-ammonia vapors mixture.

2 Analysis

The present work focus on a numerical investigation of water-ammonia condensation on a falling binary liquid film inside a

parallel plate condenser by mixed convection. The parallel condenser is composed by two parallel vertical plates ([Figure 1](#)). One of the plates is wetted and cooled by the thermal flux cooling while the other plate is isothermal and dry. The falling mixture liquid enters the first plate with an inlet temperature T_{OL} , inlet mass flow rate m_{OL} and inlet liquid composition of ammonia $c_{Liq, ammonia}$. The air enters the channel with an inlet temperature T_0 , water and ammonia vapour concentrations c_{O1} and c_{O2} and inlet velocity u_0 .

2.1 Assumptions

For mathematical formulation of the problem, the following simplifying assumptions are taken into consideration:

- Vapour mixture is ideal.
- The boundary layer approximation are valuable.
- Dufour and Soret effects are negligible.
- Viscous dissipation and radiative heat transfer are negligible.
- Liquid mixture is ideal.
- Flows and transfers in the two phases are steady, laminar and two-dimensional.
- The effect of the superficial tension is negligible. The gas-liquid interface is thermodynamic equilibrium.

2.2 Governing equations

The equations governing the flow and coupled mass and heat transfers in the liquid and in the gas phases are as follows ([Siow et al., 2002](#); [Le et al., 2022](#)).

For the film condensate.

Continuity equation:

$$\frac{\partial \rho_L u_L}{\partial x} + \frac{\partial \rho_L v_L}{\partial y} = 0 \tag{1}$$

x-momentum equation:

$$\rho_L \left(u_L \frac{\partial u_L}{\partial x} + v_L \frac{\partial u_L}{\partial y} \right) = \rho_L g - \frac{dp}{dx} + \frac{\partial}{\partial y} \left(\mu_L \frac{\partial u_L}{\partial y} \right) \tag{2}$$

Energy equation:

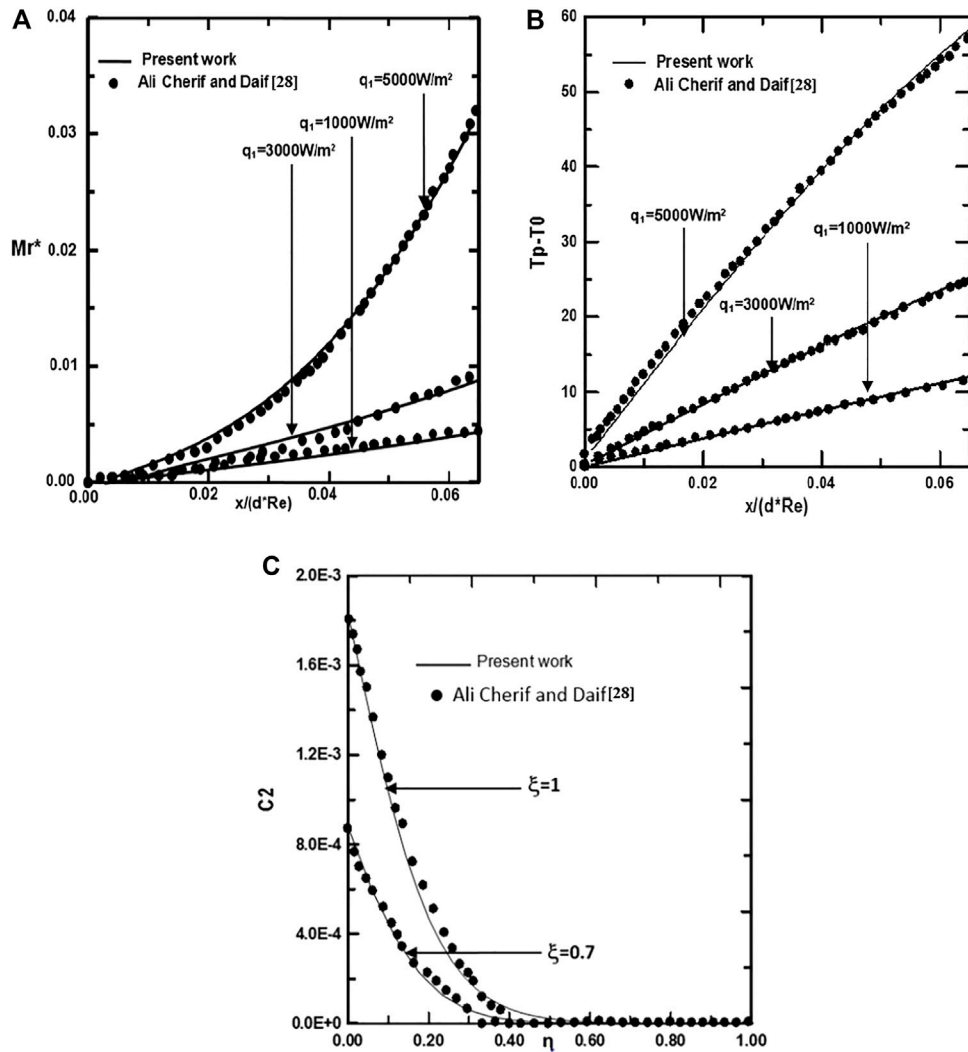


FIGURE 2 Validation of calculated total evaporating rate along the channel (A), interfacial temperature (B) and the concentration of ethylene glycol vapor along the channel (C): C_{Liq} , ethylene glycol = $C_{Liq, water} = 0.5$, (50% water-ethylene glycol mixture).

$$\rho_L c_{pL} \left(u_L \frac{\partial T_L}{\partial x} + v_L \frac{\partial T_L}{\partial y} \right) = \frac{\partial}{\partial y} \left(\lambda_L \frac{\partial T_L}{\partial y} \right) + \rho_L D_L (c_{pL,1} - c_{pL,2}) \frac{\partial T_L}{\partial y} \frac{\partial c_{L1}}{\partial y} \quad (3)$$

Species diffusion equation:

$$u_L \frac{\partial c_{Li}}{\partial x} + v_L \frac{\partial c_{Li}}{\partial y} = \frac{1}{\rho_L} \frac{\partial}{\partial y} \left(\rho_L D_L \frac{\partial c_{Li}}{\partial y} \right) \quad i = 1, 2 \quad (4)$$

Overall mass equation:

$$\int_0^\delta \rho_L u_L dy = m_{oL} + \int_0^x \rho v(x, 0) dx \quad (5)$$

For the gaseous phase.

Continuity equation:

$$\frac{\partial \rho u}{\partial x} + \frac{\partial \rho v}{\partial y} = 0 \quad (6)$$

x-momentum equation:

$$u \frac{\partial u}{\partial x} + v \frac{\partial u}{\partial y} = -\frac{1}{\rho} \frac{dP}{dx} - \beta g (T - T_0) - g \sum_{i=1}^2 \beta_i^* (c_i - c_{i0}) + \frac{1}{\rho} \frac{\partial}{\partial y} \left(\mu \frac{\partial u}{\partial y} \right) \quad (7)$$

Energy equation:

$$\rho c_p \left(u \frac{\partial T}{\partial x} + v \frac{\partial T}{\partial y} \right) = \frac{\partial}{\partial y} \left(\lambda \frac{\partial T}{\partial y} \right) + \rho \sum_{i=1}^2 (D_{g,im} c_{pi} - D_{g,am} c_{pa}) \frac{\partial T}{\partial y} \frac{\partial c_i}{\partial y} \quad (8)$$

Species diffusion equation:

$$u \frac{\partial c_i}{\partial x} + v \frac{\partial c_i}{\partial y} = \frac{1}{\rho} \frac{\partial}{\partial y} \left(\rho D_{g,im} \frac{\partial c_i}{\partial y} \right) \quad i = 1, 2, 3 \quad (9)$$

Where $c_1 + c_2 + c_3 = 1$.

Overall mass equation:

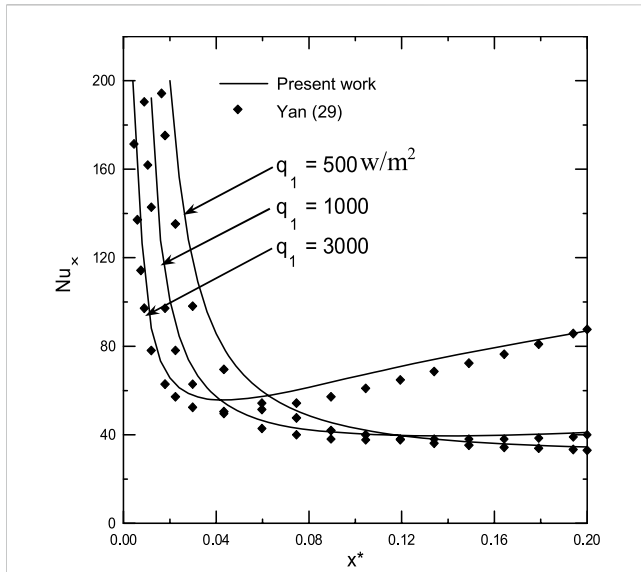


FIGURE 3
Validation of calculated local Nusselt number Nu_x at the interface liquid-gas.

$$\int_{\delta}^d \rho u dy = (d - \delta) \rho_0 u_0 + \int_0^x \rho v(x, 0) dx \quad (10)$$

2.3 Boundary conditions

- At $x = 0$ (for the inlet conditions):

$$u = u_0; T(0, y) = T_0; P = P_0; c_i(0, y) = c_{0i} \quad (11)$$

$$u = u_0; T(0, y) = T_0; P = P_0 \text{ and } c_i(0, y) = c_{0i}$$

$$T_L(0, y_L) = T_{0L}; m(0, y_L) = m_{0L}; c_{Li, ammonia} = c_{L0} \quad (12)$$

- At $y = d$ (for the dry plate):

$$v(x = d, y) = 0; u(x = d, y) = 0; \frac{\partial c_i}{\partial y} = 0; T(x = d, y) = T_W \quad (13)$$

- At $y_L = 0$ (For the wet plate):

$$u_L(x, 0) = v(x, 0) = 0; q_1 = -\lambda_L \left. \frac{\partial T_L}{\partial y_L} \right|_{y_L=0}; \left. \frac{\partial c_{Li}}{\partial y_L} \right|_{y_L=0} = 0 \quad (14)$$

- At $y_L = \delta$ and $y = 0$ (For the gas-liquid interface):

The continuities of velocities and temperatures are:

$$u_L(x, y_L = \delta) = u(x, y = 0); T_L(x, y_L = \delta) = T(x, y = 0) \quad (15)$$

The transversal velocity is:

$$v(x, y = 0) = \frac{\sum_{i=1}^2 D_{g,im} \frac{\partial c_i}{\partial y} \Big|_{y=0}}{1 - \sum_{i=1}^2 c_i(x, y = 0)} \quad (16)$$

The continuities of shear stress and local condensation rate of species i give:

$$\mu_L \left. \frac{\partial u_L}{\partial y_L} \right|_{\eta_i=1} = \mu \left. \frac{\partial u}{\partial y} \right|_{y=0}; \dot{m}_i = \dot{m}_{c_{Li}} - \rho_L D_{L,i} \left. \frac{\partial c_{Li}}{\partial y_L} \right|_{y_L=\delta} = \dot{m}_{c_i} - \rho D_{g,im} \left. \frac{\partial c_i}{\partial y} \right|_{y=0} \quad (17)$$

The heat balance at the interface implies:

$$-\lambda_L \left. \frac{\partial T_L}{\partial y_L} \right|_{y_L=\delta} = -\lambda \left. \frac{\partial T}{\partial y} \right|_{y=0} - \dot{m} L_v \quad (18)$$

2.4 Equation transformation

In order to fix the position of the liquid gas interface, we introduce the following transformations (Figure 1B):

In the gaseous phase:

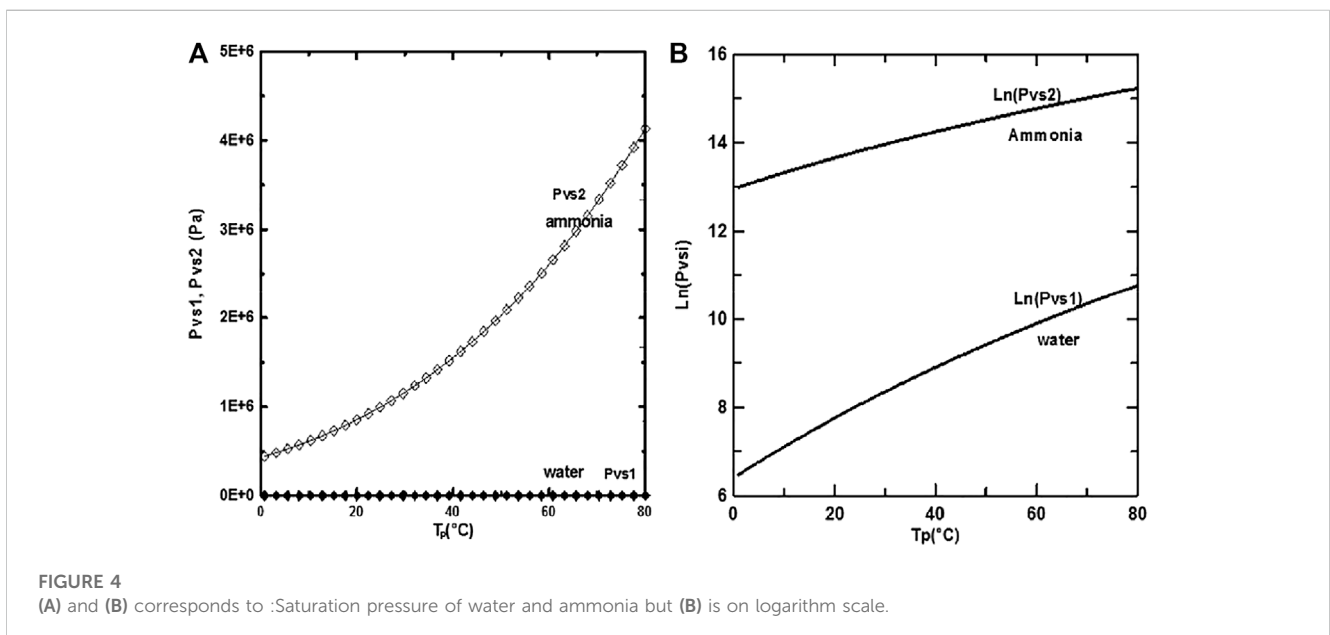


FIGURE 4
(A) and (B) corresponds to : Saturation pressure of water and ammonia but (B) is on logarithm scale.

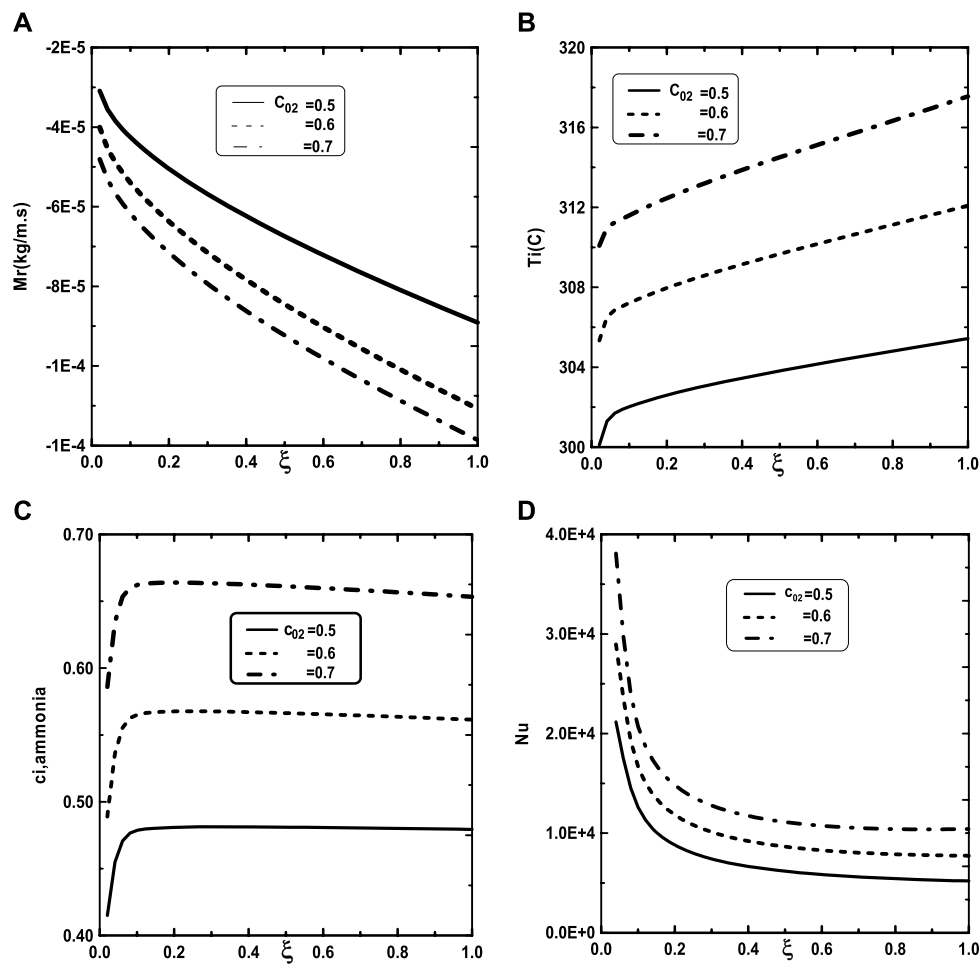


FIGURE 5 Effect of the inlet vapor concentration of ammonia c_{02} on the cumulated condensation rate of vapors mixture (A), the interfacial temperature (B), the ammonia vapor concentration (C) and the Nusselt number (D): $c_{01} = 0.3$, $T_{0L} = 10^\circ\text{C}$, $T_0 = 20^\circ\text{C}$, $T_w = 20^\circ\text{C}$, $q_1 = 0$, $m_{0L} = 0.001 \text{ kg/m.s}$, $c_{Liq, ammonia} = 0.5$ (50% water-ammonia mixture).

$$\eta = (y - \delta(d - \delta)), \xi = x/H$$

$$\frac{\partial}{\partial y} = \frac{1}{d - \delta(x)} \frac{\partial}{\partial \eta} \text{ and } \frac{\partial}{\partial x} = \frac{1}{H} \frac{\partial}{\partial \xi} + \frac{\eta - 1}{(d - \delta(x))H} \frac{\partial \delta}{\partial \xi} \frac{\partial}{\partial \eta}$$

In the liquid phase:

$$\eta_L = y/\delta, \xi = x/H$$

$$\frac{\partial}{\partial y} = \frac{1}{\delta(x)} \frac{\partial}{\partial \eta_L}$$

and

$$\frac{\partial}{\partial x} = \frac{1}{H} \frac{\partial}{\partial \xi} - \frac{\eta_L}{\delta(x)H} \frac{\partial \delta}{\partial \xi} \frac{\partial}{\partial \eta_L}$$

2.4.1 For the Liquid Phase

Continuity equation:

$$\frac{\partial \rho_L u_L}{\partial \xi} - \frac{\eta_L}{\delta} \frac{\partial \delta}{\partial \xi} \frac{\partial \rho_L u_L}{\partial \eta_L} + \frac{H}{\delta} \frac{\partial \rho_L v_L}{\partial \eta_L} = 0 \tag{19}$$

x-momentum equation:

$$u_L \frac{\partial u_L}{\partial \xi} + \left(v_L \frac{H}{\delta} - u_L \frac{\eta_L}{\delta} \frac{\partial \delta}{\partial \xi} \right) \frac{\partial u_L}{\partial \eta_L} = -\frac{1}{\rho_L} \frac{dP}{d\xi} - \frac{H}{\rho_L \delta^2} \frac{\partial}{\partial \eta_L} \left[\mu_L \frac{\partial u_L}{\partial \eta_L} \right] + gH \tag{20}$$

Energy equation:

$$u_L \frac{\partial T_L}{\partial \xi} + \left(u_L \frac{\eta_L - 1}{\delta} \frac{\partial \delta}{\partial \xi} + \frac{H}{\delta} v_L \right) \frac{\partial T_L}{\partial \eta_L} = \frac{1}{\rho_L C_{pL}} \left\{ \frac{H}{(\delta)^2} \frac{\partial}{\partial \eta_L} \left(\lambda_L \frac{\partial T_L}{\partial \eta_L} \right) + \rho_L D_L (C_{pL,1} - C_{pL,2}) \frac{H}{(\delta)^2} \frac{\partial T_L}{\partial \eta_L} \frac{\partial c_{L,1}}{\partial \eta_L} \right\} \tag{21}$$

Species diffusion equation:

$$u_L \frac{\partial c_{Li}}{\partial \xi} + \left(u_L \frac{\eta_L - 1}{\delta} \frac{\partial \delta}{\partial \xi} + \frac{H}{\delta} v_L \right) \frac{\partial c_{Li}}{\partial \eta_L} = \frac{1}{\rho_L} \frac{H}{\delta^2} \frac{\partial}{\partial \eta_L} \left(\rho_L D_{Li} \frac{\partial c_{Li}}{\partial \eta_L} \right); \tag{22}$$

$i = 1, 2$

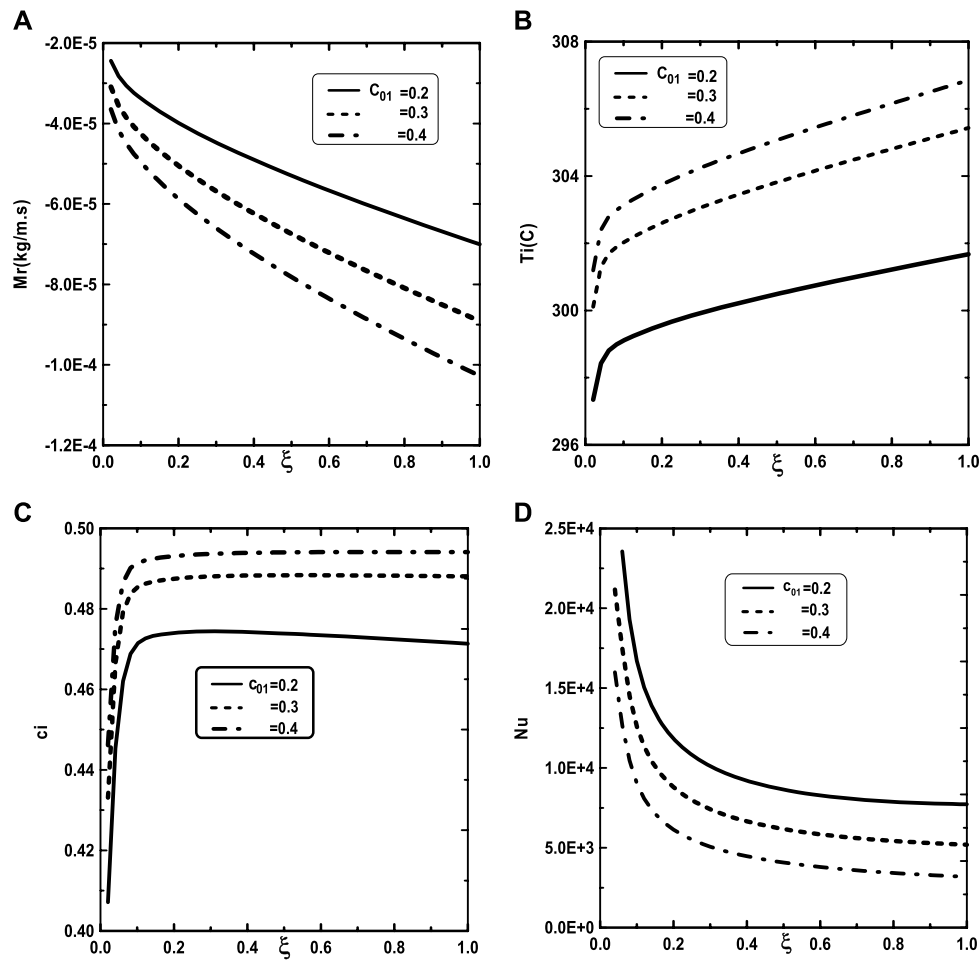


FIGURE 6 Effect of the inlet vapor concentration of water c_{01} on the cumulated condensation rate of vapors mixture (A), the interfacial temperature (B), the ammonia vapor concentration (C) and the Nusselt number (D): $c_{02} = 0.5$, $T_{0L} = 10^\circ\text{C}$, $T_0 = 20^\circ\text{C}$, $T_w = 20^\circ\text{C}$, $q_1 = 0$, $m_{0L} = 0.001 \text{ kg/m.s}$, $c_{\text{Liq, ammonia}} = 0.5$ (50% water-ammonia mixture).

Overall mass balance:

$$\int_0^1 \delta \rho_L u_L d\eta_L = \left[m_{0L} - H \int_0^\xi \rho v(\xi, \eta = 0) d\xi \right] \quad (23)$$

$$u \frac{\partial T}{\partial \xi} + \left(u \frac{\eta - 1}{d - \delta} \frac{\partial \delta}{\partial \xi} + \frac{H}{d - \delta} v \right) \frac{\partial T}{\partial \eta} = \frac{1}{\rho C_p} \left\{ \frac{H}{(d - \delta)^2} \frac{\partial}{\partial \eta} \left(\lambda \frac{\partial T}{\partial \eta} \right) + \rho \sum_{i=1}^2 (D_{g,im} c_{pi} - D_{g,am} c_{pa}) \frac{H}{(d - \delta)^2} \frac{\partial T}{\partial \eta} \frac{\partial c_i}{\partial \eta} \right\} \quad (26)$$

2.4.2. For the gas phase

Continuity equation:

$$\frac{\partial \rho u}{\partial \xi} + \frac{\eta - 1}{d - \delta} \frac{\partial \delta}{\partial \xi} \frac{\partial \rho u}{\partial \eta} + \frac{H}{d - \delta} \frac{\partial \rho v}{\partial \eta} = 0 \quad (24)$$

x-momentum equation:

$$u \frac{\partial u}{\partial \xi} + \left(\frac{\eta - 1}{d - \delta} \frac{\partial \delta}{\partial \xi} u + \frac{H}{d - \delta} v \right) \frac{\partial u}{\partial \eta} = -\frac{1}{\rho} \frac{dP}{d\xi} - g\beta H (T - T_0) - gH \sum_{i=1}^2 \beta_i^* (c_i - c_{0i}) + \frac{1}{\rho} \frac{H}{(d - \delta)^2} \frac{\partial}{\partial \eta} \left(\mu \frac{\partial u}{\partial \eta} \right) \quad (25)$$

Energy equation:

Species diffusion equation:

$$u \frac{\partial c_i}{\partial \xi} + \left(u \frac{\eta - 1}{d - \delta} \frac{\partial \delta}{\partial \xi} + \frac{H}{d - \delta} v \right) \frac{\partial c_i}{\partial \eta} = \frac{1}{\rho} \frac{H}{(d - \delta)^2} \frac{\partial}{\partial \eta} \left(\rho D_{g,im} \frac{\partial c_i}{\partial \eta} \right); \quad i = 1, 2 \quad (27)$$

Overall mass balance:

$$\int_0^1 \rho (d - \delta) u(\xi, \eta) d\eta = \left[(d - \delta_0) \rho_0 u_0 + H \int_0^\xi \rho v(\xi, \eta = 0) d\xi \right] \quad (28)$$

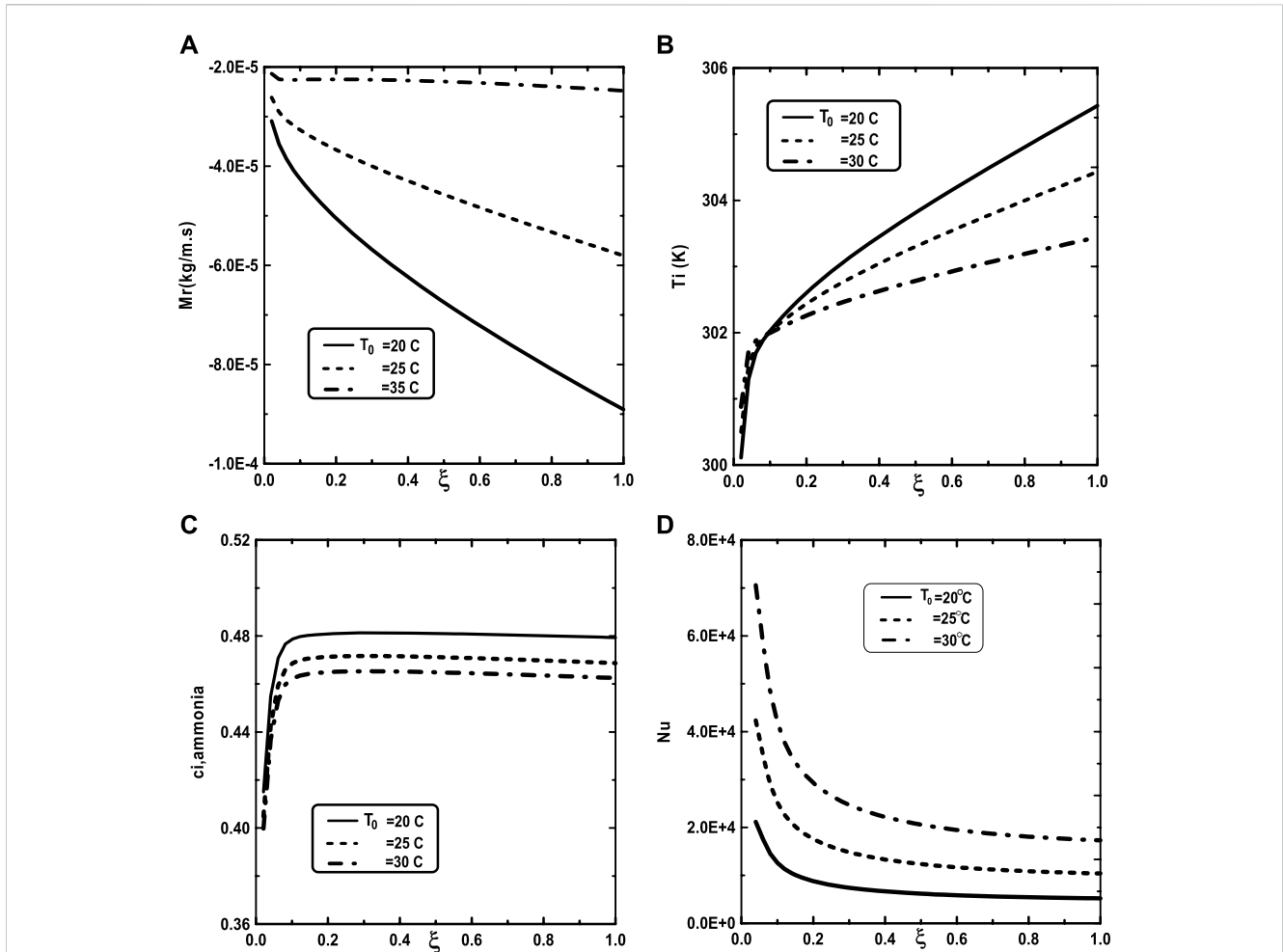


FIGURE 7 Effect of the inlet gas temperature T_0 on the cumulated condensation rate of vapors mixture (A), the interfacial temperature (B), the ammonia vapor concentration (C) and the Nusselt number (D): $c_{O1} = 0.3$, $c_{O2} = 0.5$, $T_{OL} = 10^\circ\text{C}$, $T_w = 20^\circ\text{C}$, $q_1 = 0$, $m_{0L} = 0.001 \text{ kg/m.s}$, $c_{Li,q, ammonia} = 0.5$ (50% water-ammonia mixture).

2.4.3. Boundary conditions

* For $\xi = 0$ (for the inlet conditions):

$$T(0, \eta) = T_0; c_i(0, \eta) = c_{oi}; u(0, \eta) = u_0; p(0, \eta) = p_0 \quad (29)$$

$$T_L(0, \eta_L) = T_{OL}; m(0, \eta_L) = m_{OL}; c_{Li}(0, \eta_L) = c_{OLi} \quad (30)$$

* At $\eta = 1$ (dry plate):

$$u(\xi, 1) = 0 = v(\xi, 1); T(\xi, 1) = T_w; \left. \frac{\partial c_i}{\partial \eta} \right|_{\eta=1} = 0 \quad (31)$$

* At $\eta_L = 0$ (wet plate):

$$u_L(\xi, 0) = 0; v_L(\xi, 1) = 0; q_1 = -\lambda_L \left. \frac{\partial T_L}{\partial \eta_L} \right|_{\eta_L=0}; \left. \frac{\partial c_{Li}}{\partial \eta_L} \right|_{\eta_L=0} = 0 \quad (32)$$

* At $\eta = 0$ ($\eta_L = 1$) (gas-liquid interface):

$$u_L(\xi, \eta_L = 1) = u(\xi, \eta = 0); T_L(\xi, \eta_L = 1) = T(\xi, \eta = 0) \quad (33)$$

$$v(\xi, \eta = 0) = -\frac{\frac{1}{d-\delta} \sum_{i=1}^2 D_{g,im} \frac{\partial c_i}{\partial \eta}}{1 - \sum_{i=1}^2 c_i(\xi, \eta = 0)} \quad (34)$$

$$\left. \frac{1}{\delta} \mu_L \frac{\partial u_L}{\partial \eta_L} \right|_{\eta_L=1} = \frac{1}{d-\delta} \left. \frac{\partial u}{\partial \eta} \right|_{\eta=0}; \dot{m}_i = \dot{m} c_{Li} - \left. \frac{\rho_i D_{Li}}{\delta} \frac{\partial c_{Li}}{\partial \eta_L} \right|_{\eta_L=0} = \dot{m} c_i - \left. \frac{\rho D_{g,im}}{d-\delta} \frac{\partial c_i}{\partial \eta} \right|_{\eta=0} \quad (35)$$

$$-\left. \frac{1}{\delta} \lambda_L \frac{\partial T_L}{\partial \eta_L} \right|_{\eta_L=1} = -\left. \frac{1}{d-\delta} \lambda \frac{\partial T}{\partial \eta} \right|_{\eta=0} - \dot{m} L_v \quad \text{with} \quad \dot{m} = -\frac{\frac{1}{d-\delta} \rho \sum_{i=1}^2 D_{g,im} \frac{\partial c_i}{\partial \eta}}{1 - \sum_{i=1}^2 c_i(\xi, \eta = 0)} \quad (36)$$

In order to evaluate the importance of the different processes of energy transfer, the following quantities are used:

- The cumulated condensation rate of species I vapor at the interface is given by:

$$Mr_i(x) = \int_0^\xi \dot{m}_i(\xi) d\xi \quad \text{where} \quad \dot{m}_i(\xi) = \dot{m} c_i - \left. \frac{\rho D_{g,im}}{d-\delta} \frac{\partial c_i}{\partial \eta} \right|_{\eta=0} \quad (37)$$

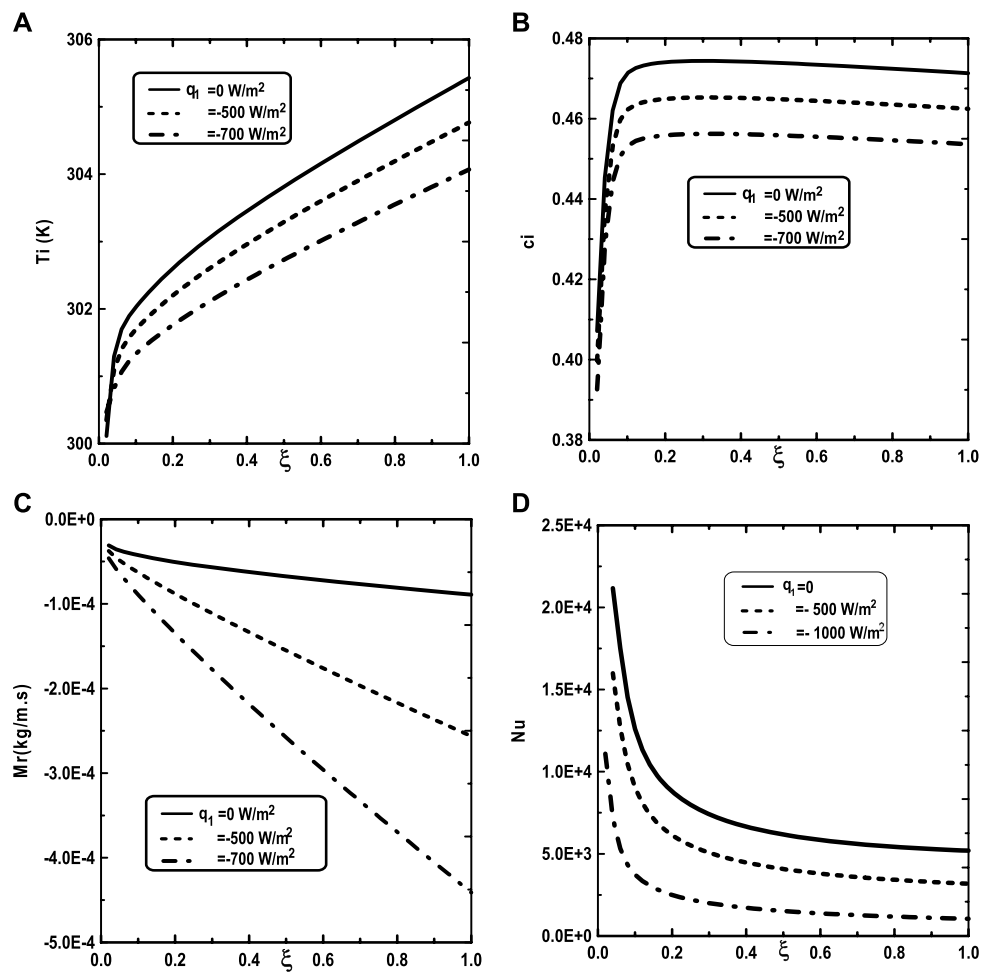


FIGURE 8 Effect of the heat flux q_1 on the cumulated condensation rate of vapors mixture (A), the interfacial temperature (B), the ammonia vapor concentration (C) and the Nusselt number (D): $c_{O1} = 0.3$, $c_{O2} = 0.5$, $T_{OL} = 10^\circ\text{C}$, $T_w = 20^\circ\text{C}$, $T_0 = 20^\circ\text{C}$, $m_{0L} = 0.001 \text{ kg/m.s}$, $c_{\text{Liq, ammonia}} = 0.5$ (50% water-ammonia mixture).

- The cumulated condensation rate of vapor mixture at the interface is given by:

$$Mr = \int_0^\xi \dot{m}_i(\xi) d\xi = Mr_1 + Mr_2 \quad (38)$$

3 Solution method

The system of partial differential Equations and its boundary and interfacial conditions (1–19) was solved using FORTRAN code with the implicit finite difference method. The governing partial differential equations was transformed into finite difference equations by using a fully implicit marching scheme. The mesh is characterized by a longitudinal step $\Delta\xi = 1/(N_\xi - 1)$ and a transversal step $\Delta\eta_L = 1/(N_{\eta L} - 1)$ in liquid and $\Delta\eta = 1/(N_\eta - 1)$ in gas. The axial convection terms were approximated by the upstream difference and the transverse convection and diffusion terms by the central difference is

employed to transform the governing equations into finite difference equations. The system of finite equations was solved by the Gaussian elimination method. To confirm that the results were grid-independent, we present in Table 1 the stability of calculation from the mesh variations local evaporation rate $\dot{m}(X)$. Table 1 shows that the difference in the local evaporation rate obtained using $51 \times (51 + 31)$ and $151 \times (51 + 51)$ grids was less than 1%.

To check the adequacy of the numerical scheme adopted in the present study, the procedure has been tested by comparing the total evaporating rate (Mr), the interfacial temperature ($T_p - T_0$) and the concentration of ethylene glycol vapour calculated from the present code with the results of Ali Cherif (Ali and Daif, 1999) for the case of the evaporation of the binary (water-ethylene glycol) liquid film flowing down on one plate of the vertical channel (see Figures 2A–C). The first plate of a vertical channel is wetted by the binary liquid film and externally subjected to a uniform heated flux q_1 while the second ($y = d$) is dry and adiabatic. The comparison has been done for $T_0 = 293.15\text{K}$, $c_{O1} = c_{O2} = 0$, $T_{OL} = 293.15\text{K}$, $q_2 = 0$,

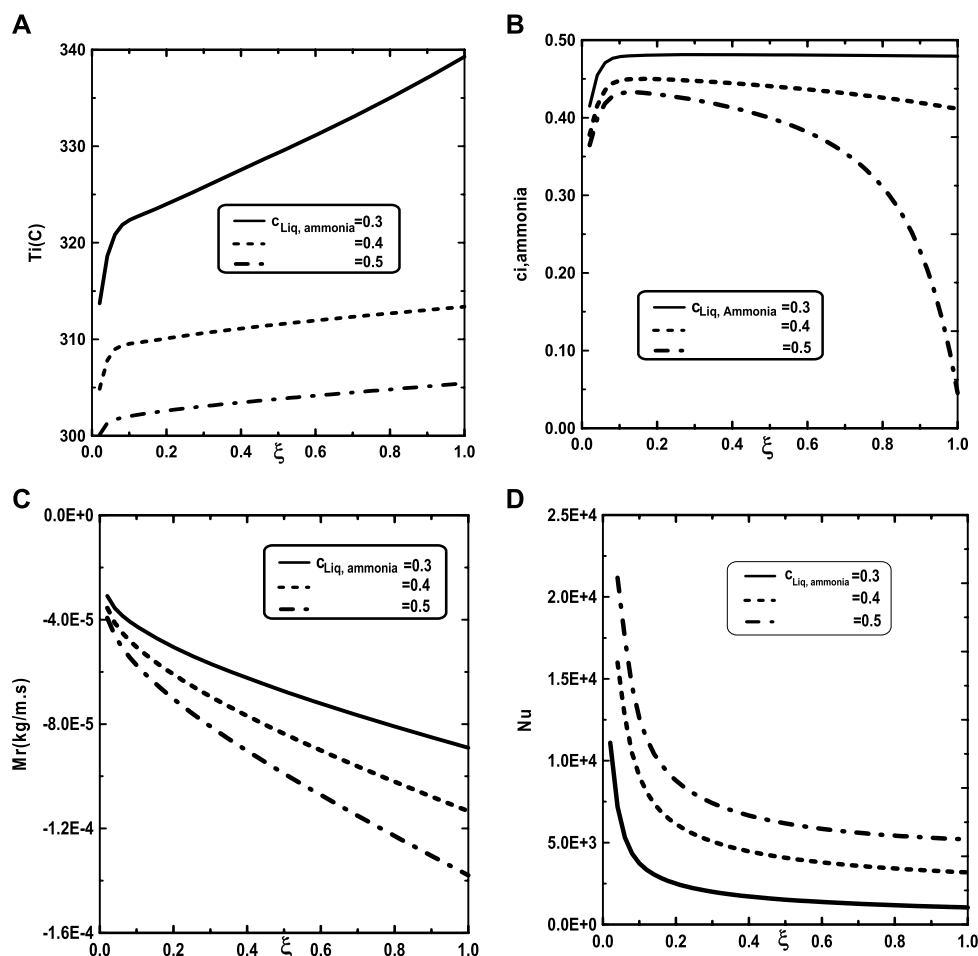


FIGURE 9 Effect of inlet liquid concentration of ammonia $c_{Liq, ammonia}$ on the interfacial temperature (A), the ammonia vapor concentration (B), the cumulated condensation rate of vapors mixture (C) and the Nusselt number (D): $c_{O1} = 0.3$, $c_{O2} = 0.5$, $q_1 = 0$, $T_{OL} = 10^\circ\text{C}$, $T_w = 20^\circ\text{C}$, $T_0 = 20^\circ\text{C}$, $m_{OL} = 0.001 \text{ kg/m.s}$.

$m_{OL} = 0.02 \text{ Kg/m.s}$, $Re = 1,000$, the geometrical ratio is $d/H = 0.015$, the imposed wall heat flux is $q_1 = 3000 \text{ W/m}^2$ and the inlet film composition of ethylene glycol is $c_{Liq, ethylene glycol} = 0.5$ (50% water-ethylene glycol mixture). Figures 2A–C show a satisfactory conformity between our results and those obtained by Ali Cherif and Daif (Ali and Daif, 1999). The second validation of the numerical scheme adopted in the present study has been carried out in the case of evaporation of pure water liquid film under mixed convection. The water liquid film is falling down on one plate of a vertical channel. The first plate of a vertical channel is wetted by the liquid film and externally subjected to a uniform heated flux q_1 while the second ($y = d$) is dry and adiabatic. The comparison between our results and those obtained in the literature by Yan (1992) has been done for $T_0 = 293.15\text{K}$, $c_0 = 0$, $\phi_0 = 50\%$, $T_{OL} = 293.15\text{K}$, $q_2 = 0$, $Re = 2000$, $d/H = 0.015$, $q_1 = 1000\text{W/m}^2$. The procedure has been tested by comparing the local Nusselt number Nu_x at the interface to those of Yan (1992). Concerning the comparison of the local Nusselt number Nu_x , the inlet flow rate $m_{OL} = 0.02 \text{ Kg/m.s}$. Figure 3 shows a satisfactory conformity between our results and those obtained by Yan (Yan, 1992).

4 Results and discussions

The study results were attained with the following values: $d/H = 0.015$, $u_0 = 0.75 \text{ m/s}$, and $P_0 = 9 \text{ bars}$. The saturation pressure of ammonia is more significant than that of water, as seen in Figures 4A, B and as a result, ammonia is more volatile than water. It is shown from Figure 3 A, B that the difference between the saturation pressures of ethylene-glycol and water is observed to grow increasingly significant as the wall temperature increases.

4.1 Effects of the inlet parameters in the gas phase and the thermal flux cooling

Figure 5 illustrates the effect of the inlet ammonia vapor concentration on the vapors mixture condensation, the interfacial temperature, the ammonia vapor concentration at the interfacial and the Nusselt number. In fact, Figure 5A shows that the vapors mixture condensation is enhanced for

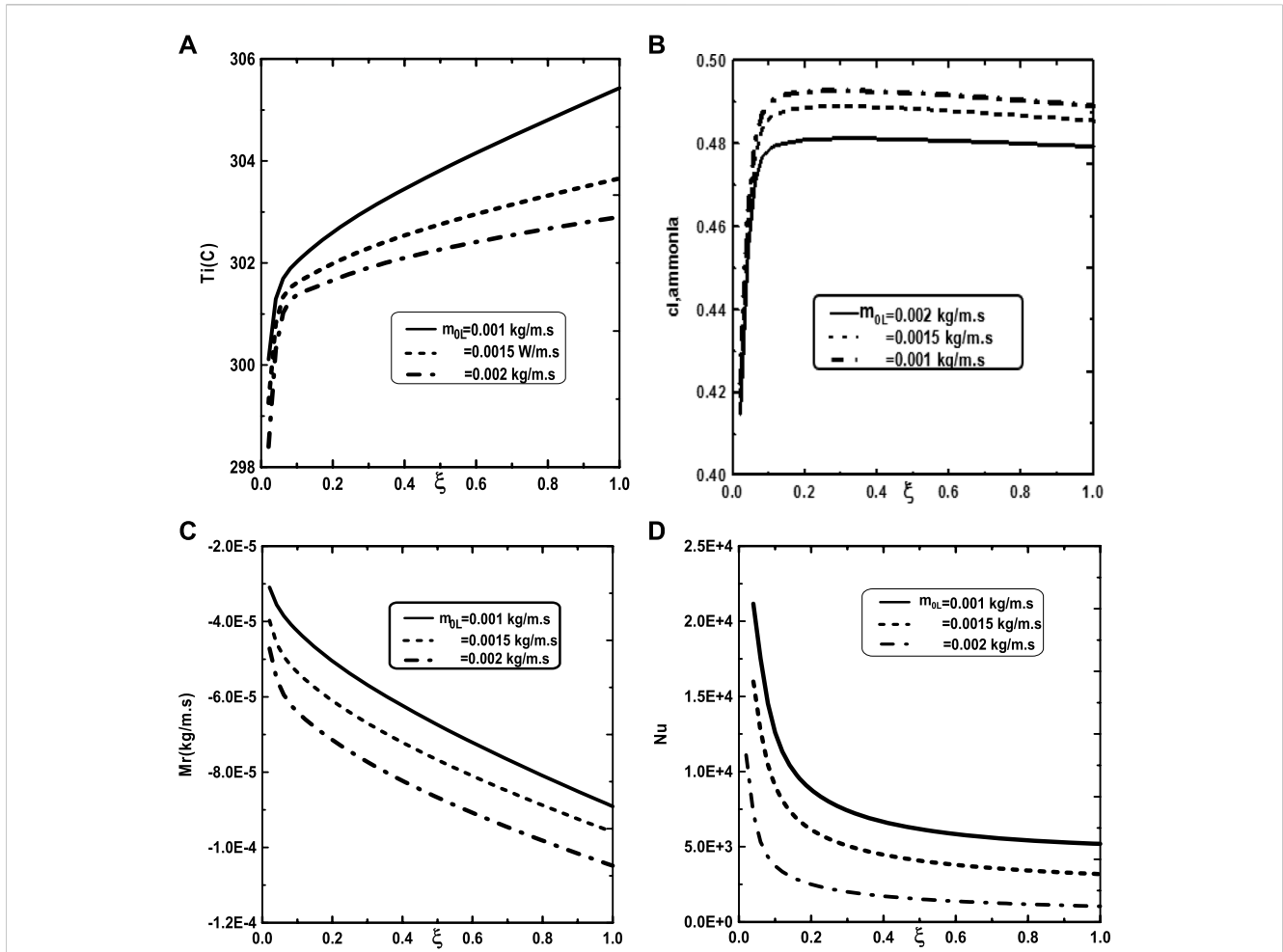


FIGURE 10 Effect of inlet liquid mass flow rate m_{0L} on the interfacial temperature (A), the ammonia vapor concentration (B), the cumulated condensation rate of vapors mixture (C) and the Nusselt number (D): $c_{O1} = 0.3$, $c_{O2} = 0.5$, $q_1 = 0$, $T_{OL} = 10^\circ\text{C}$, $T_w = 20^\circ\text{C}$, $T_0 = 20^\circ\text{C}$, $c_{Liq, ammonia} = 0.5$ (50% water-ammonia mixture).

higher inlet ammonia vapor concentration. This result is due to the fact that an augmentation of the inlet ammonia vapor concentration c_{O2} causes an intensification of the ammonia vapor amount in the gas which will be condensable to the liquid film. As the inlet gas temperature T_0 rises, one can observe that the temperature at the liquid-gas interface also increase (Figure 5B). This results have been explained by the fact that an increasing of the mixture condensation is accompanied by an increase of temperature at the liquid-gas interface. It is obvious, from Figure 5C, that an augmentation of the ammonia vapour concentration at the channel entry increases its values at the liquid-gas interface. Figure 5D shows that the increase in the inlet vapor concentration of ammonia c_{O2} improves the heat transfer. This results is manifested by an increase in the Nusselt number Nu when we increase the inlet vapor concentration of ammonia c_{O2} . Figure 6 illustrate the effect of inlet vapour concentration of water c_{O1} on the cumulated condensation rate of vapors mixture, the temperature at the liquid-gas interface, the ammonia vapor concentration at the liquid-gas interface and the Nusselt number. Figure 6A shows that the mixture condensation is enhanced with an increase of inlet vapour

concentration of water c_{O1} causing an increase in the temperature (Figure 6B) and vapor ammonia concentration (Figure 6C) at the liquid-gas interface. It is shown from Figure 6D that an increase in the inlet vapor concentration of water c_{O1} induces an increase of the Nusselt number Nu causing an enhancement in the heat transfer. Figure 7 give the evolution of the axial distribution of the cumulated condensation rates and the temperature, vapour ammonia concentration at the interface liquid-gas with different values of inlet gas temperature T_0 and on the Nusselt number. The observation of the curves of Figure 7A shows that a decrease of inlet gas temperature T_0 advantages the vapors mixture condensation causing an elevation in the temperature (Figure 7B) and vapor ammonia concentration (Figure 7C) the interface liquid-gas. It is shown from Figure 7D that the Nusselt number Nu is increased when the inlet gas temperature T_0 is elevated. The effect of the density of thermal flux cooling q_1 on the heat and mass transfer and on the vapors mixture condensation rate is given in the Figure 8. Figure 8A reveals a decrease of the interfacial temperature when the density of thermal flux cooling q_1 increases. The same behaviour has been observed in Figure 8B and it's

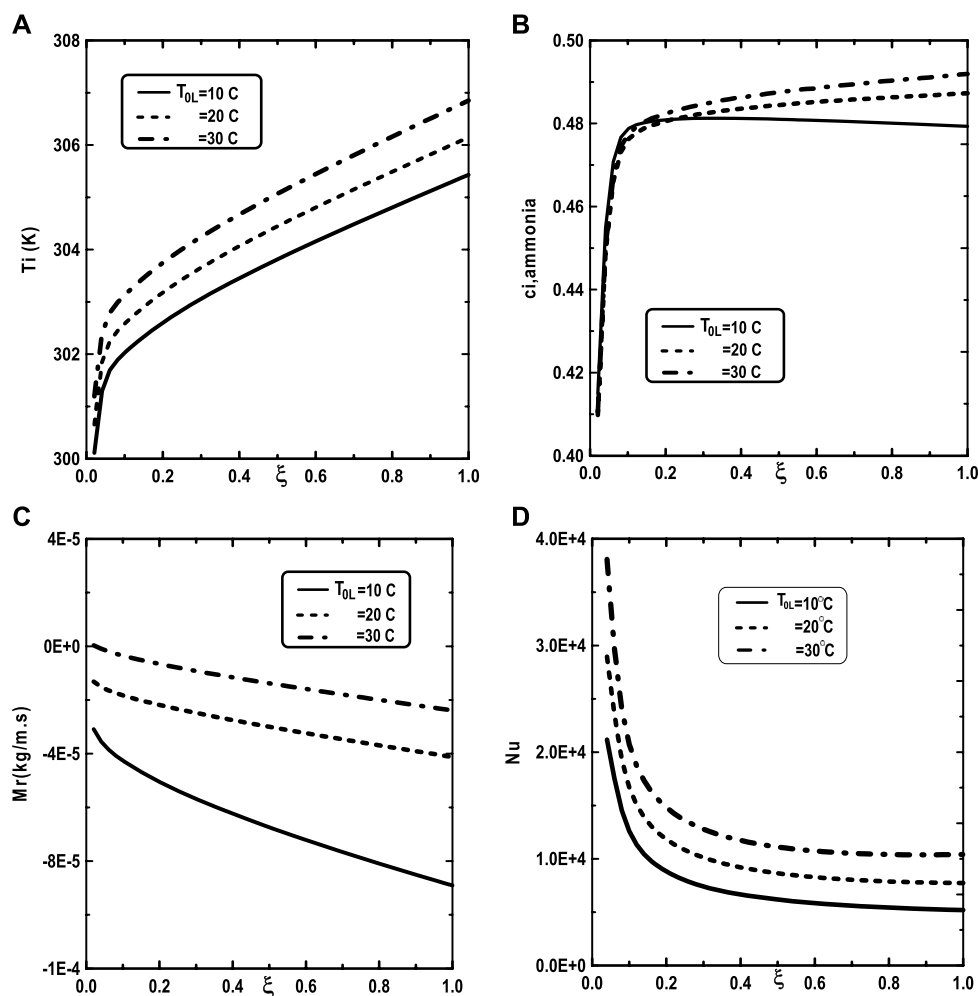


FIGURE 11 Effect of inlet liquid temperature T_{0L} on the interfacial temperature (A), the ammonia vapor concentration (B), the cumulated condensation rate of vapors mixture (C) and the Nusselt number (D): $c_{O1} = 0.3$, $c_{O2} = 0.5$, $q_1 = 0$, $T_w = 20^\circ\text{C}$, $T_0 = 20^\circ\text{C}$, $C_{\text{Liq, ammonia}} = 0.5$ (50% water-ammonia mixture), $m_{0L} = 0.001\text{ kg/m.s}$

shown that the density of thermal flux cooling q_1 induces an increase in the vapor ammonia concentration at the liquid-gas interface. It is found from Figure 8C that the vapors mixture condensation is enhanced with an elevation of thermal flux cooling q_1 . This results can be justified by the fact than an increase of q_1 ameliorates the cooling at the liquid-gas interface which causing an enhancement of vapors mixture condensation. It is found from Figure 8D that the Nusselt number Nu is decreased when the cooling heat flux q_1 is elevated.

4.2 Effect of the inlet properties of the binary liquid film

In Figure 9, one presented the impact of binary liquid film composition on the temperature and vapor ammonia concentration, the vapors mixture condensation and on the Nusselt number. Figure 9A shows that when the inlet liquid concentration of ammonia $C_{\text{Liq, ammonia}}$

increase, the interfacial temperature decrease causing a decrease in the vapor ammonia concentration at the liquid-gas interface. This results can be explained by the fact that an increase of inlet liquid concentration of ammonia $C_{\text{Liq, ammonia}}$ causing an increase in the volatility of the binary liquid (the ammonia is more volatile than the water) and consequently enhances the interface liquid cooling. The decrease of the temperature at the interface liquid-gas causing a decrease in the vapor ammonia concentration at the interface liquid-gas (Figure 9B). It's shown from Figure 9C that an augmentation in the inlet liquid concentration of ammonia $C_{\text{Liq, ammonia}}$ improves the vapors mixture condensation. This result is due to the fact that an increase in the inlet liquid concentration of ammonia $C_{\text{Liq, ammonia}}$ benefits the liquid-gas interface cooling causing an amelioration in the vapors mixture condensation. Figure 9D indicates that the Nusselt number Nu is decreased when the inlet liquid concentration of ammonia $C_{\text{Liq, ammonia}}$ is elevated.

We turn our attention now to the impact of the inlet flow rate m_{0L} of liquid film and the inlet liquid temperature T_{0L} on the temperature and vapor ammonia concentration at the interface liquid-gas, the

vapors mixture condensation and on the Nusselt number. Figure 10A shows that the increase of the inlet flow rate m_{0L} of liquid film advantages the cooling at the interface liquid-gas. The observation of the curves of Figure 10B shows that the vapor ammonia concentration at the interface liquid-gas is elevated for the high value of inlet flow rate m_{0L} . Figure 10C reveals that a significant increase of the vapors mixture condensation when the inlet flow rate m_{0L} increases. This results have been explained by the fact that an increase in the inlet flow rate advantages the cooling at the interface liquid-gas causing an augmentation in the vapors mixture condensation. Figure 10D shows that the Nusselt number Nu is more important for the higher inlet flow rate m_{0L} . Figure 11 illustrates the influence of the inlet liquid temperature T_{0L} on the temperature at the interface liquid-gas, the vapor ammonia concentration at the liquid-gas interface and the vapors mixture condensation and the Nusselt number. As expected from Figure 11A, the interfacial temperature increase with an increase of inlet liquid temperature T_{0L} . It's shown from Figure 11B that an increase of inlet liquid temperature T_{0L} induces an increase of the vapor ammonia concentration at the interface liquid-gas. Figure 11C indicates that a lower inlet liquid temperature T_{0L} results in a lower vapors mixture condensation. This result is explained by the fact that an increase in the inlet liquid temperature T_{0L} induces an increase in the temperature at the interface liquid-gas causing an augmentation in the vapor mixture condensation. Figure 11D indicates that an increase in the inlet liquid temperature T_{0L} causes a higher Nusselt number.

5 Conclusion

The numerical investigation of binary liquid film condensation from water-ammonia vapors mixture flowing downward on a parallel plate condenser by mixed convection has been effected. The parallel plate condenser is composed by two parallel vertical plates (Figure 1). One of the plates is wetted by nanofilm liquid and cooled by the thermal flux cooling while the other plate is isothermal and dry. The influence of the inlet gas parameters, inlet liquid parameters and thermal flux cooling on the coupled heat and mass transfer and on the efficiency of the parallel plate condenser has been studied. The finding of this study can be summarized as follows:

- 1) The increase in the inlet vapor of ammonia as well as of vapor water benefits the vapors mixture condensation.
- 2) The increase in the thermal flux cooling advantages the vapors mixture condensation.
- 3) The increase in the inlet liquid flow rate enhances the vapors mixture condensation.

References

- Akiyama, H., Nagasaki, T., and Ito, Y. (2001). "Numerical analysis on the dropwise condensation of a binary vapor mixture," Proceedings of the ASME 2001 International Mechanical Engineering Congress and Exposition.
- Ali, C. A., and Daif, A. (1999). Numerical study of heat and mass transfer between two vertical flat plates in the presence of a binary liquid film flowing down on one of the heated plates. *Int. J. Heat. Mass Transf.* 42, 2399–2418.
- Yang, B., Sun, S., Fan, Y., Hu, N., and Chen, H., 2023, Numerical study of condensation film formation and transforming processes on porous surface within ceramic membrane, *Int. J. Therm. Sci.*, 183, 107850, doi:10.1016/j.ijthermalsci.2022.107850
- Berto, A., Azzolin, M., Pascal, L., Glushchuk, A., Miscevic, M., Del Col, D., et al. (2022). Experimental investigation of liquid film thickness and heat transfer during condensation in microgravity. *Int. J. Heat Mass Transf.* 199, 123467. doi:10.1016/j.ijheatmasstransfer.2022.123467
- Chang, W., Yoo, J.-S., and Cho, H. K. (2021). Multi-scale simulation of wall film condensation in the presence of non-condensable gases using heat structure-coupled CFD and system analysis codes. *Nucl. Eng. Technol.* 53, 2488–2498. doi:10.1016/j.net.2021.03.001
- Chaynane, R., Mohamed, A., Boushaba, H., Zeghamati, B., and Khmou, A. (2004). Étude de la condensation en film laminaire d'une vapeur pure et saturée sur la paroi poreuse d'une plaque inclinée. *Mech. Industry* 5, 381–391. doi:10.1051/meca:2004038

- 4) The decrease of the inlet gas temperature improves the vapors mixture condensation.
- 5) A decrease in the inlet liquid temperature ameliorates the vapors mixture condensation.
- 6) The increase in the inlet liquid concentration of ammonia (or the increase of inlet liquid concentration of water) inhibits the vapors mixture condensation.

Data availability statement

The original contributions presented in the study are included in the article/Supplementary Material, further inquiries can be directed to the corresponding author.

Author contributions

Conceptualization, ABN; Data curation, ABN; Formal analysis, AA-G; Writing—original draft, ABN; Writing—review and editing, AA-G. All authors contributed to the article and approved the submitted version.

Acknowledgments

The authors would like to thank the Deanship of Scientific Research at Umm Al-Qura University for supporting this work by Grant Code: (23UQU4340531DSR001).

Conflict of interest

The authors declare that the research was conducted in the absence of any commercial or financial relationships that could be construed as a potential conflict of interest.

Publisher's note

All claims expressed in this article are solely those of the authors and do not necessarily represent those of their affiliated organizations, or those of the publisher, the editors and the reviewers. Any product that may be evaluated in this article, or claim that may be made by its manufacturer, is not guaranteed or endorsed by the publisher.

- Chung, B. J., Kim, S., Kim, M. C., and Ahmadi, M. (2004). Experimental comparison of film-wise and drop-wise condensations of steam on vertical flat plates with the presence of air. *Int. Commun. Heat Mass Transf.* 31, 1067–1074. doi:10.1016/j.icheatmasstransfer.2004.08.004
- George, M., George, K., Constantoudis, V., Lam, C., Tripathy, A., Mitridis, E., et al. (2022). The role of shadowed droplets in condensation heat transfer. *Int. J. Heat Mass Transf.* 197, 123297. doi:10.1016/j.ijheatmasstransfer.2022.123297
- Hughes, M. T., and Chen, S. M. (2022). Srinivas Garimella, machine-learning-based heat transfer and pressure drop model for internal flow condensation of binary mixtures. *Int. J. Heat Mass Transf.* 194, 123109.
- Kuchma, A. E., Shchekin, A. K., and Kuni, F. M. (2011). Simultaneous establishing of stationary growth rate and composition of supercritical droplets at isothermal binary condensation in the diffusion-controlled regime. *Phys. A Stat. Mech. its Appl.* 390, 3308–3316. doi:10.1016/j.physa.2011.05.028
- Kuchma, A. E., Martyukova, D. S., Lezova, A. A., and Shchekin, A. K. (2013). Size, temperature and composition of a spherical droplet as a function of time at the transient stage of nonisothermal binary condensation or evaporation. *Colloids Surfaces A Physicochem. Eng. Aspects* 432, 147–156. doi:10.1016/j.colsurfa.2013.04.023
- Lee, Y., Cha, M., Kim, H., and Jo, H. (2022). Film condensation heat transfer of high-pressure and low-mass-flux steam in inclined tube. *Int. J. Heat Mass Transf.* 189, 122714. doi:10.1016/j.ijheatmasstransfer.2022.122714
- Li, K., Liu, Y., Wen, J., Wang, S., and Tu, J. (2022). A numerical model for the flow condensation of the binary zeotropic mixture. *Int. Commun. Heat Mass Transf.* 130, 105767. doi:10.1016/j.icheatmasstransfer.2021.105767
- Liu, P., Ho, J. Y., Wong, T. N., and Toh, K. C. (2020). Laminar film condensation inside and outside vertical diverging/converging small channels: A theoretical study. *Int. J. Heat Mass Transf.* 149, 119193. doi:10.1016/j.ijheatmasstransfer.2019.119193
- Merouani, L., Zeghami, B., Belhamri, A., Renken, K.-J., and Aboye, M. (1993). Experiments on film condensation promotion within thin inclined porous coatings. *Int. J. Heat. Mass Transf.* 36, 1347–1355. doi:10.1016/s0017-9310(05)80102-4
- Minkowycz, W. W. J., and Sparrows, E. M. (1969). The effect of superheating on condensation heat transfer in a forced convection boundary layer flow. *Int. J. Heat Mass Transf.* 12, 147–154. doi:10.1016/0017-9310(69)90058-1
- Nasr, A., and Al-Ghamdi, A. S. (2017). Numerical study of evaporation of falling liquid film on one of two vertical plates covered with a thin porous layer by free convection. *Int. J. Therm. Sci.* 112, 335–344. doi:10.1016/j.ijthermalsci.2016.10.018
- Nasr, A. (2018). Heat and mass transfer for liquid film condensation along a vertical channel covered with a thin porous layer. *Int. J. Therm. Sci.* 24, 288–299. doi:10.1016/j.ijthermalsci.2017.10.016
- Panday, P. K. (2003). Two-dimensional turbulent film condensation of vapours flowing inside a vertical tube and between parallel plates: A numerical approach. *Int. J. Refrig.* 26, 492–503. doi:10.1016/s0140-7007(02)00162-7
- Le, Q. T., Ormiston, S. J., and Soliman, H. M., (2022). Detailed modeling of laminar film condensation from zeotropic binary mixtures in a vertical tube. *Int. J. Heat Mass Transf.* 186, 122440. doi:10.1016/j.ijheatmasstransfer.2021.122440
- Renken, K. J., Aboye, M., Carneiro, M., and Meechan, K. (1993). Effect of vapor velocity on film condensation along a surface embedded in a porous medium. *Int. Commun. Heat Mass Transf.* 20, 1–13. doi:10.1016/0735-1933(93)90002-d
- Siow, E. C., Ormiston, S. J., and Soliman, H. M. (2002). Fully coupled solution of a two-phase model for laminar film condensation of vapor–gas mixtures in horizontal channels. *Int. J. Heat Mass Transf.* 45, 3689–3702. doi:10.1016/s0017-9310(02)00094-7
- Turkylmazoglu, M. (2017). Condensation of laminar film over curved vertical walls using single and two-phase nanofluid models. *Eur. J. Mech. - B/Fluids* 65, 184–191. doi:10.1016/j.euromechflu.2017.04.007
- Varier, A. S., Joshi, M., and Swaminathan, J. (2022). Improved air gap distillation desalination through induced film condensation. *Energy Convers. Manag.* 258, 115545. doi:10.1016/j.enconman.2022.115545
- Wang, J., Li, J. M., and Hwang, Y. (2018). Modeling of film condensation flow in oval microchannels. *Int. J. Heat Mass Transf.* 126, 1194–1205. doi:10.1016/j.ijheatmasstransfer.2018.05.126
- Wang, J., Li, Y., Ma, Z., Chen, N., and Li, G. (2020). Condensate droplet growth characteristics of Marangoni condensation of ethanol–water mixtures on a horizontal surface. *Int. J. Heat Mass Transf.* 160, 120170. doi:10.1016/j.ijheatmasstransfer.2020.120170
- Wu, J., Sun, X., Xue, L., and Liu, Y. (2020). Research on film condensation heat transfer at the inside of spiral coil tube. *Int. J. Heat Mass Transf.* In press. doi:10.1016/j.ijheatmasstransfer.2019.118891
- Yan, W. M. (1992). Effects of film evaporation on laminar mixed convection heat and mass transfer in a vertical channel. *Int. J. Heat. Mass Transf.* 35, 3419–3429. doi:10.1016/0017-9310(92)90228-k
- Zheng, S., Eimann, F., Philipp, C., Tobias, F., and Gross, U. (2019). Dropwise condensation in the presence of non-condensable gas: Interaction effects of the droplet array using the distributed point sink method. *Int. J. Heat Mass Transf.* 141, 34–47. doi:10.1016/j.ijheatmasstransfer.2019.06.068

Glossary

c_i	mass fraction for species i vapor
c_{pa}	specific heat for air ($J.kg^{-1}.K^{-1}$)
c_{pv}	specific heat of mixture vapour ($J.kg^{-1}.K^{-1}$)
c_{pvi}	specific heat of species i vapour ($J.kg^{-1}.K^{-1}$)
d	channel width (m)
$D_{g,am}$	mass diffusivity of dry air in the gas mixture ($m^2.s^{-1}$)
D_{Li}	mass diffusivity of species i the liquid mixture ($m^2.s^{-1}$)
c_{Li}	mass fraction for species i in the liquid film ($c_{L1} + c_{L2} = 1$)
$c_{Li, ammonia}$	inlet liquid concentration of ethylene glycol in the liquid mixture
\dot{m}_i	local condensation rate of species i ($kg.s^{-1}.m^{-2}$)
\dot{m}	local condensation rate of mixture ($\dot{m} = \dot{m}_1 + \dot{m}_2$) ($kg.s^{-1}.m^{-2}$)
u	axial velocity ($m.s^{-1}$)
v	transverse velocity ($m.s^{-1}$)

Greek symbols

Λ	thermal conductivity of the fluid ($W.m^{-1}.K^{-1}$)
M	dynamic viscosity of the fluid ($kg.m^{-1}.s^{-1}$)
Δ	thickness of liquid film (m)
ρ	density of the gas ($kg.m^{-3}$)
η	dimensionless coordinate in the transverse direction
η_L	dimensionless transverse coordinate in the liquid
ξ	dimensionless coordinate in the flow direction
β	thermal expansion coefficient $-1/\rho(\partial\rho/\partial T)_{p,c}$ (K^{-1})
β^*	mass expansion coefficient $-1/\rho(\partial\rho/\partial c)_{p,T}$

Subscripts

0	inlet condition
L	liquid